GEOPHYSICS, VOL. 57, NO. 9 (SEPTEMBER 1992); P. 1138–1154, 13 FIGS.

Iterative asymptotic inversion in the acoustic approximation

Gilles Lambaré*, Jean Virieux‡, Raul Madariaga*, and Side Jin*

ABSTRACT

We propose an iterative method for the linearized prestack inversion of seismic profiles based on the asymptotic theory of wave propagation. For this purpose, we designed a very efficient technique for the downward continuation of an acoustic wavefield by ray methods. The different ray quantities required for the computation of the asymptotic inverse operator are estimated at each diffracting point where we want to recover the earth image. In the linearized inversion, we use the background velocity model obtained by velocity analysis. We determine the short wavelength components of the impedance distribution by linearized inversion of the seismograms observed at the surface of the model. Because the inverse operator is not exact, and because the source and station distribution is limited, the first iteration of our asymptotic inversion technique is not exact. We improve the images by an iterative procedure. Since the background velocity does not change between iterations, there is no need to retrace rays, and the same ray quantities are used in the iterations. For this reason our method is very fast and efficient. The results of the inversion demonstrate that iterations improve the spatial resolution of the model images since they mainly contribute to the increase in the short wavelength contents of the final image. A synthetic example with one-dimensional (1-D) velocity background illustrates the main features of the inversion method. An example with two-dimensional (2-D) heterogeneous background demonstrates our ability to handle multiple arrivals and a nearly perfect reconstruction of a flat horizon once the perturbations above it are known. Finally, we consider a seismic section taken from the Oseberg oil field in the North Sea off Norway. We show that the iterative asymptotic inversion is a reasonable and accurate alternative to methods based on finite differences. We also demonstrate that we are able to handle an important amount of data with presently available computers.

INTRODUCTION

The construction of images of the subsurface of the earth by the inversion of seismic reflection profiles has been investigated by many authors. In a pioneering work, Cohen and Bleistein (1977) obtained an approximate solution of the inverse problem for almost vertical incidence using asymptotic methods. In a major contribution to inverse theory, Beylkin (1985) showed how to use asymptotic ray theory to construct an inverse operator for the case of a single source point and a continuous distribution of receivers on the surface of the model. Several improvements of Beylkin's original method were proposed in the literature (e.g., Miller et al., 1987; Bleistein, 1987b; Beylkin and Burridge, 1990). A common feature of these techniques is that the inverse operator was constructed by mathematical manipulation of the integral equation that relates the model to the observed seismograms. These methods are very fast because they are based on asymptotic theory. The main drawback for the construction of the asymptotic inverse operators by Beylkin's method is the need to establish a one-to-one relationship between the observed seismograms and the earth model parameters.

A very different approach to inversion, based on the theory of optimization, was proposed in a series of papers by Tarantola and coworkers (see, e.g., Tarantola, 1984; Pica et al., 1990; Crase et al., 1990). In the optimization approach, the hope of building an explicit inverse operator is abandoned and instead, an iterative method is developed to find the model that best fits observations within a certain error criterion. The optimization approach leads to algorithms that

Manuscript received by the Editor July 15, 1991; revised manuscript received January 14, 1992.
*Laboratorie de Sismologie, Université Paris 7, Institut de Physique du Globe, 75252 Paris Cedex 05, France.
‡Institut de Géodynamique, Université de Nice—CNRS, Av. Albert Einstein, 06560 Valbonne, France.

are much slower than those of Beylkin, but are much more robust and can handle incomplete and redundant data sets without problems.

Jin et al. (1992) proposed an asymptotic inversion method where the main advantages of both approaches to inversion were exploited to construct a fast and robust inversion method. In this approach, the inverse problem was formulated using classical optimization theory [see Tarantola (1987) for a recent review] but the gradient was computed using the methods of asymptotic ray theory. In their final result, Jin et al. (1992) found an iterative algorithm based on Newton's optimization method. This algorithm allows for the use of redundant and incomplete data sets, as well as for the limited frequency band of the sources used in exploration geophysics.

The inverse problem requires a very efficient algorithm for the solution of the forward problem. Most authors have adopted finite difference methods for forward modeling (see, e.g., Kolb et al., 1984; Mora, 1986; Pica et al., 1990, etc), but the computer time required by finite difference is simply too long. An alternative to finite difference is to use ray theory that is probably just as accurate as the full numerical solution in the frequency band used in vertical seismic profiling. It should be pointed out, however, that ray theory is more economical than finite differences only if ray tracing is done very efficiently. In this article, we propose an efficient downward ray-tracing strategy to compute the different parameters—traveltime, slowness vector, and geometrical spreading—required at each diffracting point by the asymptotic inverse method. We discuss the iterative asymptotic inversion described by Jin et al. (1992) in the acoustic approximation for a single parameter. It turns out that, because in linearized inversion the reference velocity model does not change, ray tracing can be done once for all the iterations. The iterations are thus run at a minimum computational cost.

In the following, we present first a synthetic example with one-dimensional (1-D) velocity background that is used to demonstrate the practical importance of iterations. A two-dimensional (2-D) background is adopted for the second synthetic example to demonstrate the use of our method in the presence of a more realistic velocity background. Finally, the acoustic algorithm will be applied to a seismic profile recorded on the North Sea, off-shore from Norway. With this example we intend to demonstrate the efficiency of our two-dimensional ray-tracing method and the importance of iterations for improving the image in a practical example.

DEPTH CONTINUATION OF ACOUSTIC FIELDS BY RAY THEORY

The high-frequency approximation of the acoustic field is required for both the forward and inverse problem. Two time scales are involved: the time of propagation and the time of the source wavelet. Using ray theory, we are able to distinguish the separate effects of these two time scales in the forward and inverse problems.

When a source has been fired at the point $\mathbf{r}_s$ with the temporal signature $S(t)$, the pressure P recorded at the point $\mathbf{r}$ outside the source area satisfies the Helmholtz equation in the frequency domain:

$$\frac{\omega^2}{c^2(\mathbf{r})} P(\mathbf{r}, \mathbf{r}_s, \omega) + \nabla^2 P(\mathbf{r}, \mathbf{r}_s, \omega) = 0, \qquad (1)$$

where c is the velocity and ∇^2 denotes the laplacian. In a 2-D medium, the high-frequency approximation to the solution of this equation is:

$$P(\mathbf{r}, \mathbf{r}_s, \omega) = S(\omega) A_0(\mathbf{r}, \mathbf{r}_s) e^{i\omega\theta(\mathbf{r},\mathbf{r}_s)} \frac{1}{\sqrt{-i\omega}}, \qquad (2)$$

where θ satisfies the eikonal equation $(\nabla\theta)^2 = c^{-2}$ and A_0 the transport equation (Červený et al., 1977). The typical tail associated with 2-D propagation arises from the term $1/\sqrt{-i\omega}$. The slowness vector $\mathbf{p} = \nabla\theta$, the gradient of θ, is perpendicular to the phase fronts $\theta = constant$. The rays, which are the orthogonal trajectories to the phase fronts, are consequently tangent to the slowness vector. Selecting a sampling parameter for phase fronts, as well as for rays, will precisely define the eikonal. We choose the sampling parameter τ, related to the traveltime by $d\theta = u^2 d\tau$, where u^2 is the square of slowness (Červený, 1987; Virieux et al., 1988; Farra et al., 1989). We always perform kinematic and dynamic or paraxial ray tracing simultaneously to be able to compute the geometrical spreading, as well as control the ray sampling inside the medium.

Starting from one point at the free surface, we sample the medium down to a specified horizon. If caustics are detected, the different ray branches (Červený et al., 1977; Hanyga, 1988) are located on this horizon and an interpolation is constructed inside each branch. After this first step, ray tracing is continued to the next horizon for each branch. With the help of interpolation, the ray may leave the horizon from any position suitable for a good discretization of the following horizon. We avoid the redundant procedure of computing branches on this new horizon starting again from the initial point. In this way, we guarantee a uniform sampling of the whole medium and avoid oversampling around the initial point and undersampling far away from the starting point. On every horizon, small ray branches may be suppressed if they are poorly sampled. A minimum of five rays are required for example to accept a ray branch. This procedure is found to be stable as long as we do not increase the number of horizons too much. A reasonable number is between two and five. Between horizons, any ray quantities needed at a sampling point are interpolated between the two rays enclosing the point for each branch.

We assume that the medium varies smoothly, a good approximation for our imaging purpose. Interfaces are not taken into account: rays between two points are always direct rays. The procedure of continuation is greatly simplified by considering only one kind of ray.

Figure 1 shows an example of ray tracing down to a horizon located at 30 km depth: no branches are observed and the horizon is uniformly sampled by the rays. In the next step, rays leave this horizon to reach the horizon down to 90 km where three branches are created. The sampling is uniform at this final horizon and it is the same as for the first horizon: consequently, the density of rays leaving this horizon is rather dense. The procedure can be repeated again for another horizon. When a branch is undersampled at a given horizon, we delete it and create an associated artificial

shadow zone coming from the downward continuation. We found that this restriction was not too severe in our practical applications.

The depth continuation by rays seems to be a very efficient technique to propagate the acoustic field downwards in a laterally heterogeneous media. Incorporating multiples will require more complex ray trajectories and was not attempted here.

ITERATIVE ASYMPTOTIC INVERSION

The iterative asymptotic inversion method that we use was discussed in a companion article (Jin et al., 1992) and is presented here in the simpler case of the acoustic approximation. A more extensive description and its extension to elastodynamics can be found in Lambaré (1991).

Born's approximation

Let us consider a 2-D medium with a velocity field described by

$$c(\mathbf{x}) = c_0(\mathbf{x}) + \Delta c(\mathbf{x}), \tag{3}$$

where $c_0(\mathbf{x})$ is a given selected velocity field and $\Delta c(\mathbf{x})$ is the perturbation of the velocity field. Although the final inverse formula will be in the time domain, discussion is easier when we proceed in the frequency domain. In this domain, the Born approximation gives a perturbation of the pressure δP at the receiver $\mathbf{r}$ for a source located at $\mathbf{r}_s$ for the velocity perturbation $\Delta c(\mathbf{x})$. We can write the pressure perturbation

$$\delta P(\mathbf{r}, \mathbf{r}_s, \omega) = \int_D dx^2\, G(\mathbf{r}, \mathbf{x}, \omega)\, \frac{-2\Delta c(\mathbf{x})}{c_0(\mathbf{x})^3}\, G(\mathbf{x}, \mathbf{r}_s, \omega)\omega^2, \tag{4}$$

where the integration domain D is over the diffracting points and $G(\mathbf{r}, \mathbf{r}', \omega)$ is the Green's function for an impulsive source at $\mathbf{r}'$ recorded at the receiver $\mathbf{r}$. This equation can be identified with equation (8) of Miller et al. (1987) by writing the perturbation

$$m(\mathbf{x}) = \frac{-2\Delta c(\mathbf{x})}{c_0(\mathbf{x})^3}, \tag{5}$$

as the function $f(\mathbf{x})$ of Miller et al. From many ways to construct Green's functions, we choose ray theory that simplifies the forward problem, as well as the inverse formulation. The Green's function is defined for an impulsive source, i.e., $S(\omega) = 1$ in equation (2). Thus for a 2-D medium we can write

$$\delta P(\mathbf{r}, \mathbf{r}_s, \omega) = \int_D dx^2\, i\omega\, m(\mathbf{x})\mathbf{A}(\mathbf{r}, \mathbf{x}, \mathbf{r}_s) e^{i\omega\tau(\mathbf{r}, \mathbf{x}, \mathbf{r}_s)}, \tag{6}$$

where $\mathbf{A}(\mathbf{r}, \mathbf{x}, \mathbf{r}_s)$ is the product of the amplitudes of the two rays connecting the source to the diffracting point and the diffracting point to the receiver. In the same way, the function τ is the sum of the two traveltimes. In the acoustic approximation with a single parameter, the summation over scattering modes given by expression (17) of Jin et al. (1992) is suppressed. We rewrite the forward problem in the compact operator expression

$$\delta P = Gm, \tag{7}$$

where $m(\mathbf{x})$ belongs to the model space M and $\delta P(\mathbf{r}, \mathbf{r}_s, \omega)$ to the data space D. G is the linearized projection operator from M into D.

The cost functional

Following Jin et al. (1992), we define the cost function

$$S(m) = 1/2\langle \delta P^{obs} - Gm | \delta P^{obs} - Gm \rangle_D, \tag{8}$$

which is defined over all the data space by the inner product

$$S(m) = 1/2 \sum_{\mathbf{r}, \mathbf{r}_s} \int_\Omega d\omega (\delta P^{obs} - Gm) Q (\delta P^{obs} - Gm), \tag{9}$$

with a weighting coefficient Q. The choice of this coefficient is based on previous works on the asymptotic approach (Beylkin, 1985; Beylkin and Burridge, 1990). This weighting kernel must correct for geometrical spreading, obliquities of rays, as well as spectral content of the asymptotic Green's function. It must also correct for the discretization of the data acquisition system whatever it is. Following Jin et al. (1992), we define the coefficient Q differently at each diffracting point $\mathbf{x}_0$, which is a rather unusual procedure for inverse problems, but is often done in migration where data

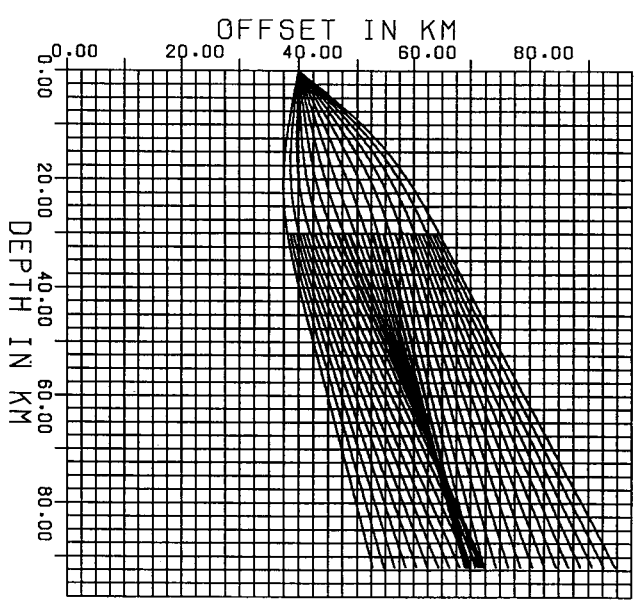

FIG. 1. Ray tracing by downward continuation between two horizons. Let us remark that the spacing between the points of arrival of the rays is the same for the two horizons. Due to defocusing, the rays in the second layer are denser than those in the second one. The initial conditions for ray shooting from the first horizon are obtained by interpolation of the rays that arrive to this interface.

are always preconditioned before migration. The expression for Q is

$$Q(r, r_s, \mathbf{x}_0, \omega) = \frac{|\mathbf{p}(r, r_s, \mathbf{x}_0)|^2}{(2\pi)^2 \omega A^2(r, \mathbf{x}_0, r_s)} J(\psi, \xi; r, r_s, \mathbf{x}_0), \tag{10}$$

where, vector $\mathbf{p} = \nabla\tau(r, r_s, \mathbf{x}_0)$ is the gradient of the two-way traveltime τ. The geometry is described by two angles. The angle ψ is the orientation of the slowness vector $\mathbf{p}$ with respect to the vertical, while the angle ξ is the aperture between the slowness vector of the source and the receiver at $\mathbf{x}_0$ (Figure 2). The Jacobian $J(\psi, \xi; r, r_s, \mathbf{x}_0)$ relates the source and station positions at the free surface to these two angles ψ and ξ at $\mathbf{x}_0$.

Asymptotic inversion

Inversion is obtained by minimizing the cost function (8) among all linearized models m. We get

$$\frac{\delta S}{\delta m} = 0 \tag{11}$$

whose solution is

$$H\langle m\rangle = G^\dagger \delta P^{obs}. \tag{12}$$

The Hessian $H = G^\dagger G$ where $G^\dagger$ is the adjoint operator to G. The right-hand side of equation (12) is recognized as the gradient γ of the cost functional with respect to the current model m. Following Jin et al. (1992), using asymptotic ray theory the gradient can be written in the very simple form:

$$\gamma(\mathbf{x}, \mathbf{x}_0) = G^\dagger \delta P^{obs}$$

$$= \frac{1}{2\pi} \sum_{r,r_s} \frac{A(\mathbf{r}, \mathbf{x}, \mathbf{r}_s)}{A^2(\mathbf{r}, \mathbf{x}_0, \mathbf{r}_s)} |\mathbf{p}|^2 J(\psi, \xi; r, r_s, \mathbf{x}_0)$$

$$\times H[\delta P^{obs}(\mathbf{r}, \mathbf{r}_s, t = \tau(\mathbf{r}, \mathbf{r}_s, \mathbf{x})] \tag{13}$$

where $H(\delta P^{obs})$ denotes the Hilbert transform of δP^{obs}. The gradient (13) is exact, but the inverse of the Hessian $H = G^\dagger G$ cannot be calculated exactly because its dimensions are too large. For this reason, we solve expression (12) by a quasi-Newton approach. Let H_a be an approximation to the Hessian H. Thus, the nth iteration of the model m is deduced from the previously obtained model by

$$\langle m_n\rangle = \langle m_{n-1}\rangle + G^{-g}[\delta P^{obs} - G\langle m_{n-1}\rangle], \tag{14}$$

where G^{-g} is the approximate generalized inverse $H_a^{-1} G^\dagger$.

An excellent approximation H_a to H can be computed using the recent work in Beylkin (1985) and Jin et al. (1991):

$$H_a(\mathbf{x}, \mathbf{x}_0) = \sum_{r,r_s} \frac{1}{(2\pi)^2} \int_\Omega d\omega\, \omega p^2 \frac{A^2(\mathbf{r}, \mathbf{x}, \mathbf{r}_s)}{A^2(\mathbf{r}, \mathbf{x}_0, \mathbf{r}_s)}$$

$$\times J(\psi, \xi; r, r_s, \mathbf{x}_0) e^{-i\omega[\tau(\mathbf{r},\mathbf{r}_s,\mathbf{x}) - \tau(\mathbf{r},\mathbf{r}_s,\mathbf{x}_0)]} \tag{15}$$

which, to first-order in $\Delta\mathbf{x} = \mathbf{x} - \mathbf{x}_0$, gives

$$H_a(\mathbf{x}, \mathbf{x}_0) = \sum_{r,r_s} \frac{1}{(2\pi)^2}$$

$$\times \int_\Omega d\omega\, \omega p^2 J(\psi, \xi; r, r_s, \mathbf{x}_0) e^{i\omega \mathbf{p}\cdot\Delta\mathbf{x}}. \tag{16}$$

We then assume that the distribution of sources and receivers is such that ξ and ψ are more or less uniformly sampled around the diffracting point $\mathbf{x}_0$. In this case, the integral in equation (16) is the approximate Fourier transform of a delta function. Uniform sampling of ξ and ψ is never obtained in practice so that the following expression is only an approximation to the Hessian.

$$H_a(\mathbf{x}, \mathbf{x}_0) = \sum_{r_s} \frac{1}{2\Delta r} \delta(\mathbf{x} - \mathbf{x}_0) = \frac{N}{2\Delta r} \delta(\mathbf{x} - \mathbf{x}_0), \tag{17}$$

where N is the number of sources and Δr is the station sampling step. For a one-parameter inversion, the effect of the aperture angle reduces to the sum over sources. Further details are given in Jin et al. (1992). Taking the initial model $\langle m_0\rangle$ as zero, the first iteration of equation (14) is

$$\langle m_1\rangle(\mathbf{x}_0) = \frac{1}{\pi} \frac{1}{N} \sum_{r,r_s} \frac{p^2}{A(\mathbf{r}, \mathbf{x}_0, \mathbf{r}_s)} J(\psi, \xi; r, r_s, \mathbf{x}_0)$$

$$\times \mathcal{H}[\delta P^{obs}(\mathbf{r}, \mathbf{r}_s, t = \tau(\mathbf{r}, \mathbf{r}_s, \mathbf{x}_0))]. \tag{18}$$

Higher order iterations of the model can be obtained from equation (14). This is done by simply replacing δP^{obs} in

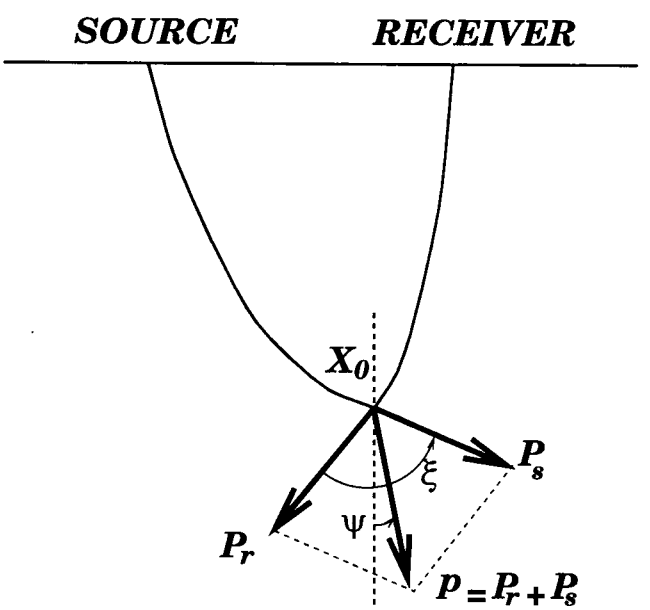

FIG. 2. Geometry of the rays connecting the source and receiver to the point $\mathbf{x}_0$ where we are currently inverting the impedance model. Vector $\mathbf{p}$ is the sum of the local slowness vectors of these two rays. The two angles ξ and ψ define the local geometry of the two rays.

equation (18) by the residual $\delta P^{obs} - G\langle m_{n-1}\rangle$. We observe that the iterative method does not require any further ray tracing because the background velocity model does not change between iterations. Thus, the traveltimes τ, amplitudes A, Jacobian J, and slowness p are the same as in the first iteration.

For the strict application of equation (18), we would need impulse-response seismograms, so that we must somehow deconvolve the recorded seismogram from the source wavelet. In practice, we used a very simple deconvolution method: the spectrum of the seismogram was divided by the spectrum of the source in the frequency range defined by the source. We did not try to do any sophisticated adaptative deconvolution, although the final image would have certainly benefited from any improvement in the low-frequency contents of the data.

The inverse expression (18) represents a stack of migrated, phase-shifted, and dynamically corrected seismograms summed over sources r_s and receivers r. The sums in the stack can be reorganized in many ways, giving different weights to different seismograms. An interesting way of processing the data is to first consider each source r_s independently. Thus we obtain several inverted vertical profiles at the same horizontal position. The set of all these vertical profiles is usually called an Iso-X section. Iso-X sections may be used very effectively to test the quality of the inversion. If the inverted profiles in an Iso-X section are similar, this is proof that the background velocity model is correct, and that the inversion has actually found an impedance profile that is coherent among several sources and receivers. Later we will show an Iso-X section for the Oseberg field data set. From the Iso-X section, we have many ways to construct an impedance model; for instance, we can choose the most energetic profile which is usually the one located right under the source. Following Jin et al. (1992), in our work we adopted the stack (18) which is a weighted sum of the different migrated profiles. The weighting, controlled by $p^2 J$, tends to eliminate the influence of wide angle reflections (large ξ) and to average the small reflection-angle profiles to obtain the final vertical profile $\langle m_1\rangle$ under every source and receiver position.

The inverse algorithm presented above is linear because we do not change the background velocity model between iterations. Of course, we might add the result of the inversion $\langle m_1\rangle$ to the reference model to generate a new background velocity model. We could then trace rays in the new reference medium and again apply the inversion algorithm (18). This nonlinear iteration has not yet been attempted because the model inverted from equation (18) and the long wavelength model used as a background are not defined over the same spatial-frequency band. How to smooth the perturbed model before adding it to the previous reference model is still an open question that we intend to discuss in a future paper.

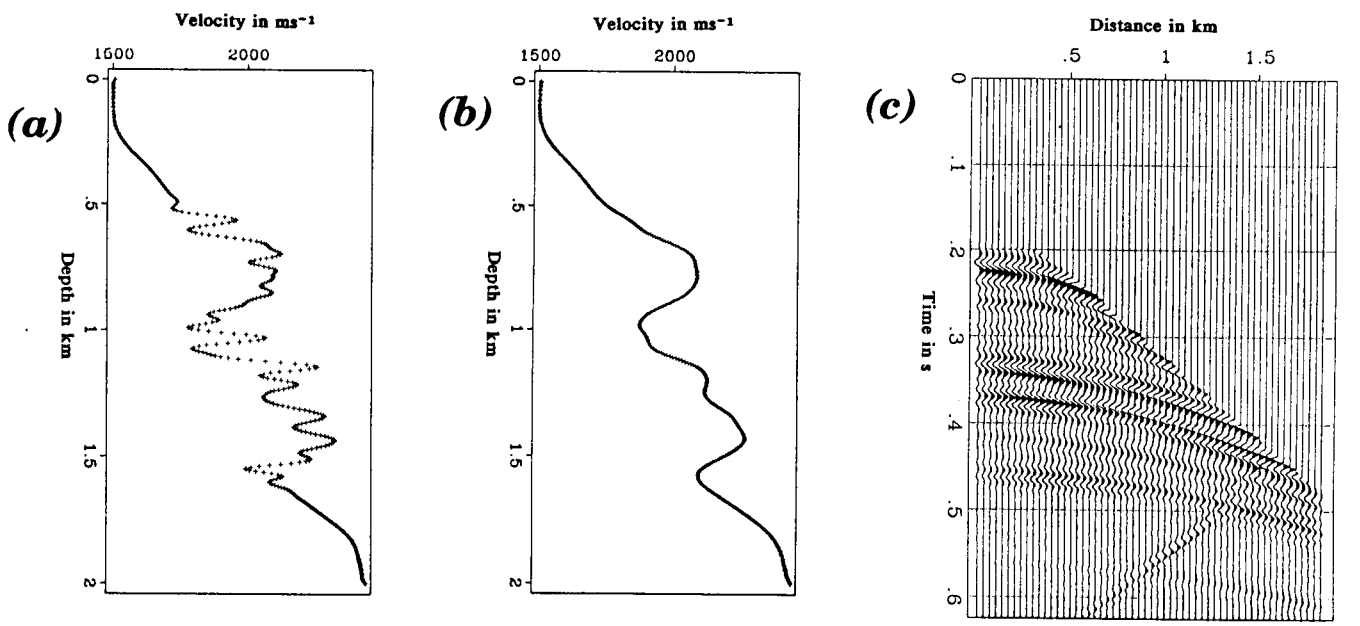

FIG. 3. Definition of a 1-D medium. In (a), we show the complete velocity model used to generate the synthetic seismograms used in the asymptotic inversion. The crosses indicate the grid points used to specify the finite-difference grid. In (b), we present the smooth profile that will be used as the background velocity for the iterative asymptotic inversion. Panel (c) shows seismograms computed by a finite-difference method with a mute applied to the direct wave, as well as to critical arrivals. Please note the weak artificial reflections coming from the numerical grid edges.

SYNTHETIC EXAMPLES TO TEST THE INVERSION PROCEDURE

Laterally uniform velocity background

To test the validity of our inversion procedure, we created a synthetic set of seismograms by the finite-difference method (Virieux, 1984) modified for the acoustic problem in Gauthier et al. (1986). We considered a 1-D medium suggested by the work of Pica (1988) and Pica et al. (1990). We discretized this velocity profile on a vertical grid of 481 points and we filtered out wavelengths shorter than 10 times the grid step. We obtained the velocity profile of Figure 3a. From this vertical profile, a low-frequency background was estimated that is also shown in Figure 3b. We used the same vertical velocity structure under each of 481 horizontal points. The spatial step of 6.67 m gives a total horizontal and vertical extension of 3200 m. The time step of 0.8 ms over 2500 steps gives a time window of 2 s. We computed synthetic seismograms for 56 receivers with a step of 33 m between receivers and a maximal offset of 1800 m (Figure 3c). The source signal was the second-order derivative of a Gaussian function $\exp(-t^2/t_c^2)$ with a characteristic time t_c of 25 ms. We have also applied a mute to get rid of the direct wave and critical arrivals.

Let us consider the low-frequency background as our initial velocity model. We performed ray tracing by the depth continuation technique with three horizons for a single source, because the reference medium is only 1-D. By means

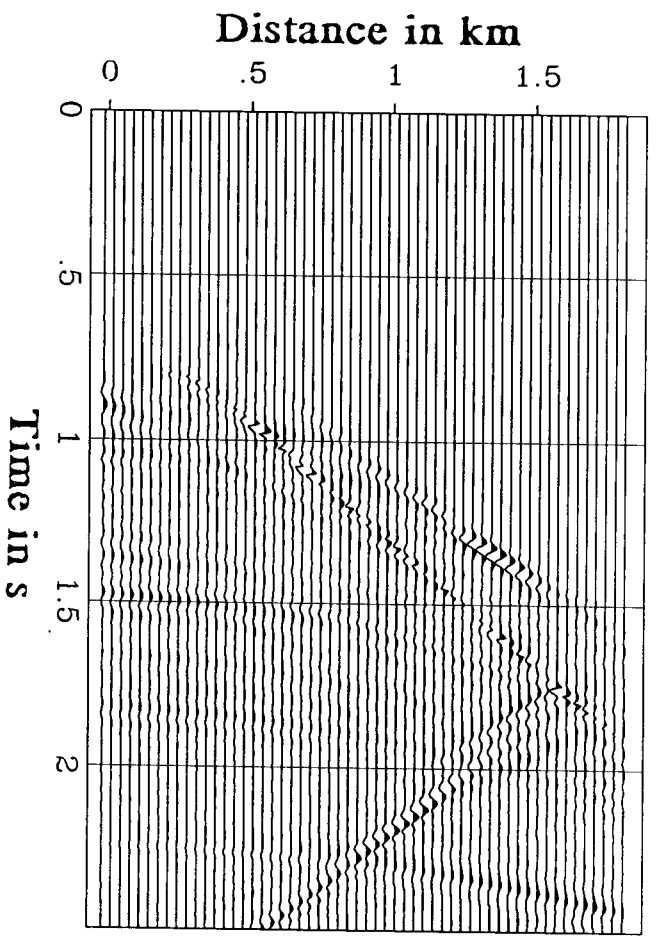

FIG. 4. Residuals of the seismograms after five iterations of the asymptotic inversion of the synthetic seismograms generated for the 1-D velocity model of Figure 3.

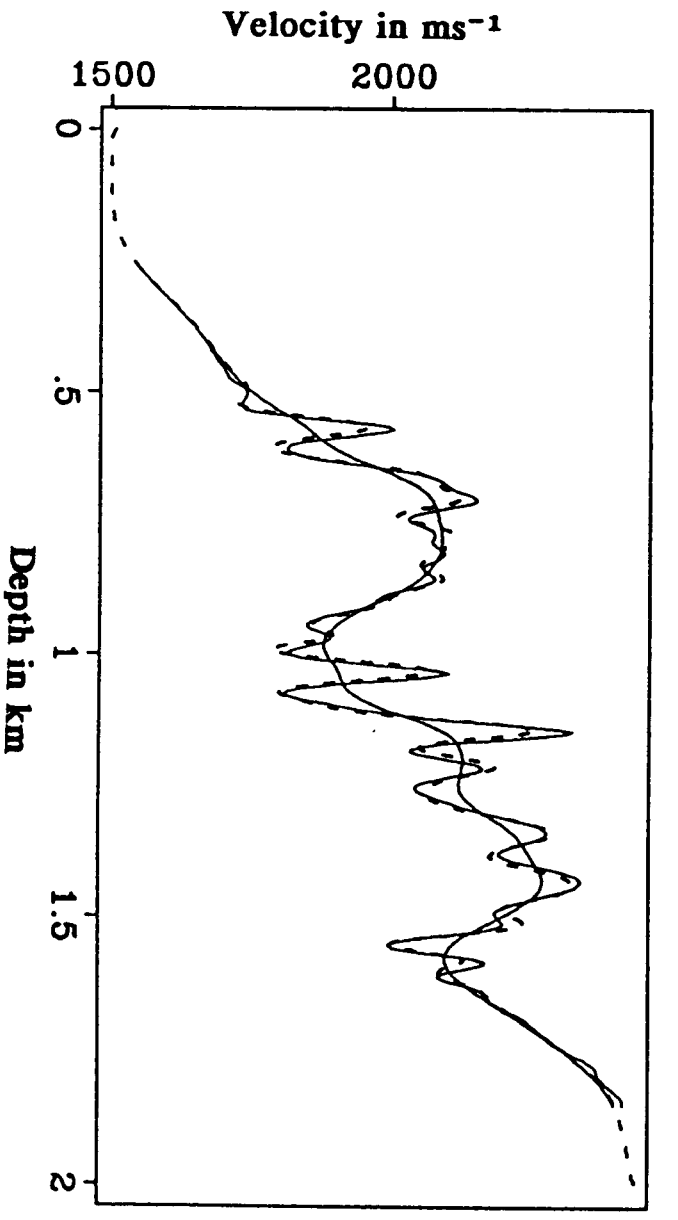

FIG. 5. Final result of the asymptotic inversion of the 1-D velocity profiles of Figure 3. The Figure shows the results of the fifth iteration. We added the background velocity before plotting the new velocity profile.

of the iterative inversion technique described above, we could improve the initial 2-D image by iterating until practically no signal was left on the residues (Figure 4), except for parasite reflections coming from the edges of the numerical grid and influences of the applied mute. A quantitative analysis is given in Figure 5, where the convergence towards a final solution is obtained in around five iterations. The "true" velocity profile is matched nearly perfectly both in positions and in amplitudes of the perturbation. We obtain the complete velocity profile by adding the background velocity to the recovered perturbation. This example is very well suited for iterative asymptotic inversion because of the high spatial-frequency band we chose to recover. Of course, as it is well understood [see Snieder et al. (1989), for example], any bias in the background velocity would have degraded the final image.

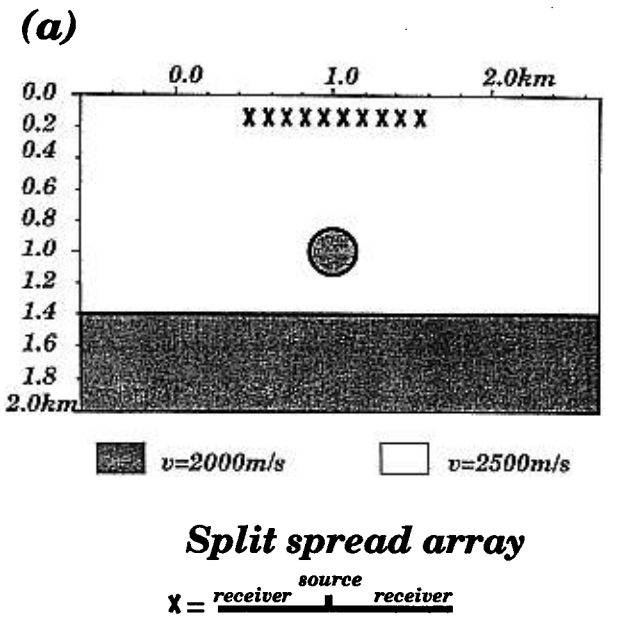

FIG. 6. (a) Geometry of the 2-D model used to test the asymptotic inversion method. The model contains a disk and a flat interface. (b) 2-D images obtained (10 shots) by asymptotic inversion of seismograms recorded at the surface of the model for a split spread array described on the top panel. Because we used an appropriate background model, the flat interface is recovered with very little deformation.

2-D velocity background

We now go one step further by taking into account lateral variations of the velocity both in the "true" model and the background model. We define a medium of velocity 2000 m/s on which we superpose a disk-like perturbation of 500 m/s located at the position $(x, z) = (1000\text{ m}, 1000\text{ m})$ with a radius of 150 m above a flat interface at a depth of 1400 m (Figure 6a). What is the image of the flat interface with the influence of the disk?

Let us assume that we have already obtained a smooth background velocity for the disk. The disk is taken into account for ray tracing, but we assume that it produces no reflections. For each source, we perform ray tracing with six reference horizons. In Figure 7, we show the rays for two sources where the influence of the disk is important and can create caustics. The precision of the inverted image increases with the number of sources. In Figure 6b, the circular shape of the disk is very well recovered, and the interface below the disk is almost horizontal; smiles have practically disappeared. In other words, time shifts associated with the disk have been correctly taken into account.

The iterative asymptotic inversion produces a very accurate high-frequency image of the subsurface. We show that the depth continuation of acoustic waves by rays is well adapted to seismic inversion and permits us to consider heterogeneous background velocities. By iteration, we were able to estimate the high frequency component of the amplitude perturbation. The deconvolution of the source wavelet is the main limiting factor to inversion. Any recovered low frequency will increase the quality of the image. The receiver distribution has a less dramatic effect and might be partially counter-balanced by the redundancy of the data.

2.5-D approximation

Before considering real data, which will be our next step, we must consider the approximation for a 3-D medium with an invariance along the y-direction. This approximation is called the "2.5-D" approximation (Bleistein, 1987a); this approach retains the ease of ray tracing in a 2-D medium, but includes the geometrical spreading of a 3-D medium, as well as a correcting factor around the diffraction point.

The geometrical spreading for this 2.5-D geometry is deduced from paraxial ray tracing. As previously shown in Bleistein (1987a), we have the relation

$$J_{2.5\text{-D}}(\tau) = J_{2\text{-D}}(\tau)\,\frac{\tau - \tau_0}{c_0(\mathbf{x})}, \tag{19}$$

which is related to the amplitude variation by the usual condition for energy conservation along ray tubes; $A_0^2(\tau)u(\tau)J(\tau)$ is kept constant along rays.

The second effect of the invariance along the y-coordinate appears in the estimation of the scattered pressure that is given in a 3-D medium by the integral

$$\delta P(\mathbf{r}, \mathbf{r}_s \omega) \simeq \omega^2 \int_D dx\ dy\ dz\ m(\mathbf{x}) A(\mathbf{r}, \mathbf{x}, \mathbf{r}_s) e^{i\omega\tau(\mathbf{r},\mathbf{x},\mathbf{r}_s)} \tag{20}$$

over the 3-D domain D of diffracting points. Sources and receivers are in the $y = 0$ plane. In this geometry, the main contribution to integral (20) comes from the vicinity of the $y = 0$ plane. We can use a stationary phase approximation for the integral along y. We find

$$\delta P(\mathbf{r}, \mathbf{r}_s \omega) \simeq \omega^{1.5} \sqrt{i2\pi}$$

$$\times \int_{y=0} dx\ dz\ m(\mathbf{x}) \frac{A(\mathbf{r}, \mathbf{x}, \mathbf{r}_s)}{(\partial\tau^2/\partial^2 y)_{y=0}} e^{i\omega\tau(\mathbf{r},\mathbf{x},\mathbf{r}_s)} \tag{21}$$

for the 2.5-D Born approximation which leads to the same inverse procedure than for the 2-D geometry except that real seismograms are processed by a different transformation $\mathcal{K}$ than the Hilbert transformation $\mathcal{H}$ of equation (18). Following Bleistein (1987a), the second partial derivative of the function τ with respect to the coordinate y is readily obtained from ray tracing and is equal to

$$\left(\frac{\partial\tau^2}{\partial^2 y}\right)_{y=0} = \frac{1}{\tau(\mathbf{r}_s, \mathbf{x})} + \frac{1}{\tau(\mathbf{r}, \mathbf{x})}, \tag{22}$$

where τ is the sampling parameter we are using during ray tracing. We are back to an expression similar to equation (6), to which we apply the asymptotic inversion method proposed in Jin et al. (1992).

INVERSION OF THE OSEBERG PROFILE NH82-269

Up to now, we have considered only synthetic data. With a 2-D seismic profile over the Oseberg Field in the North Sea off Norway, we are concerned with more than 800 shots with a total cable length of 2500 m for 96 groups of geophones. The recording time window is 6 s with a sampling step of 4 ms giving us more than 3200 millions of bits of raw data. This data set belongs to an experimental 3-D marine line.

The Oseberg Field is a large oil and gas accumulation located on the Bergen High in the transition zone between the Viking Trough to the West and the Horda Platform to the East. A general structural interpretation was given by Badley et al. (1984). A more specific description can be found in Nipen (1987) who gives a precise interpretation of the Brent Group, the reservoir for the Oseberg Field.

We preprocessed the data set to eliminate multiples coming from the sea water with a thickness of 110 m in the area. Then we deconvolved the source time signal by the following, rather simple technique. To build the deconvolution filter, we inverted the spectrum of the source in the frequency band where source spectral amplitude was large, and band-pass filtered the rest of the spectrum. The time domain deconvolution filter was finally computed by an inverse Fourier transform. We assumed that the source signal is known and is the same for the different shots.

Starting from an initial background velocity (Figure 8) obtained by standard velocity analysis and given to us with the data set, we inverted the whole profile taking only every eight sources and using the 2.5-D approximation for the

(text continued on p. 1148)

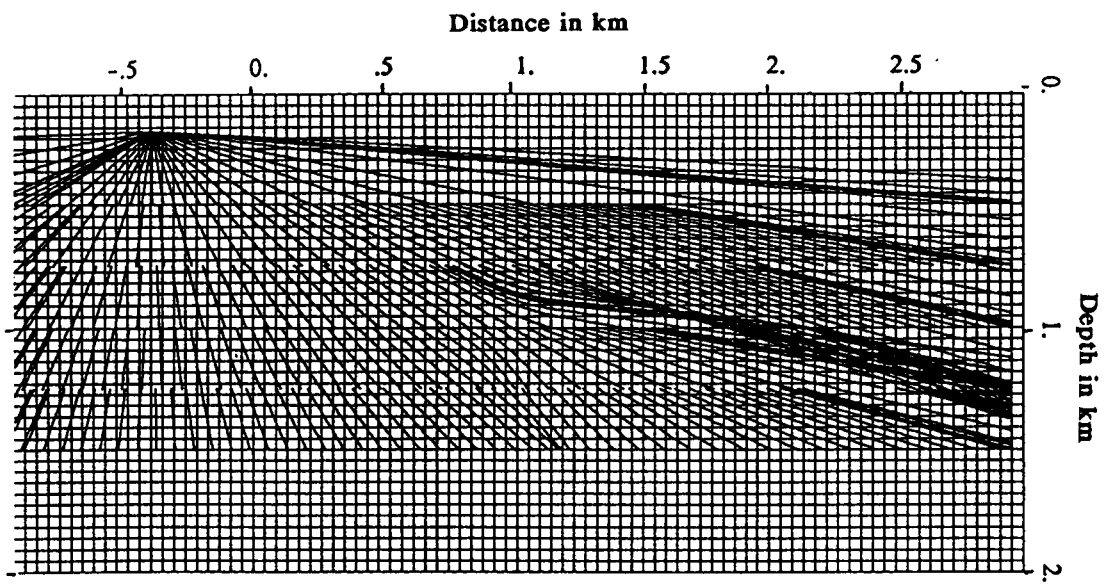

FIG. 7. Typical example of ray tracing in the heterogeneous background model of Figure 6. The shot point is the left-most point of the source array in Figure 6a. Note the formation of a caustic associated to the tangential illumination of the disk.

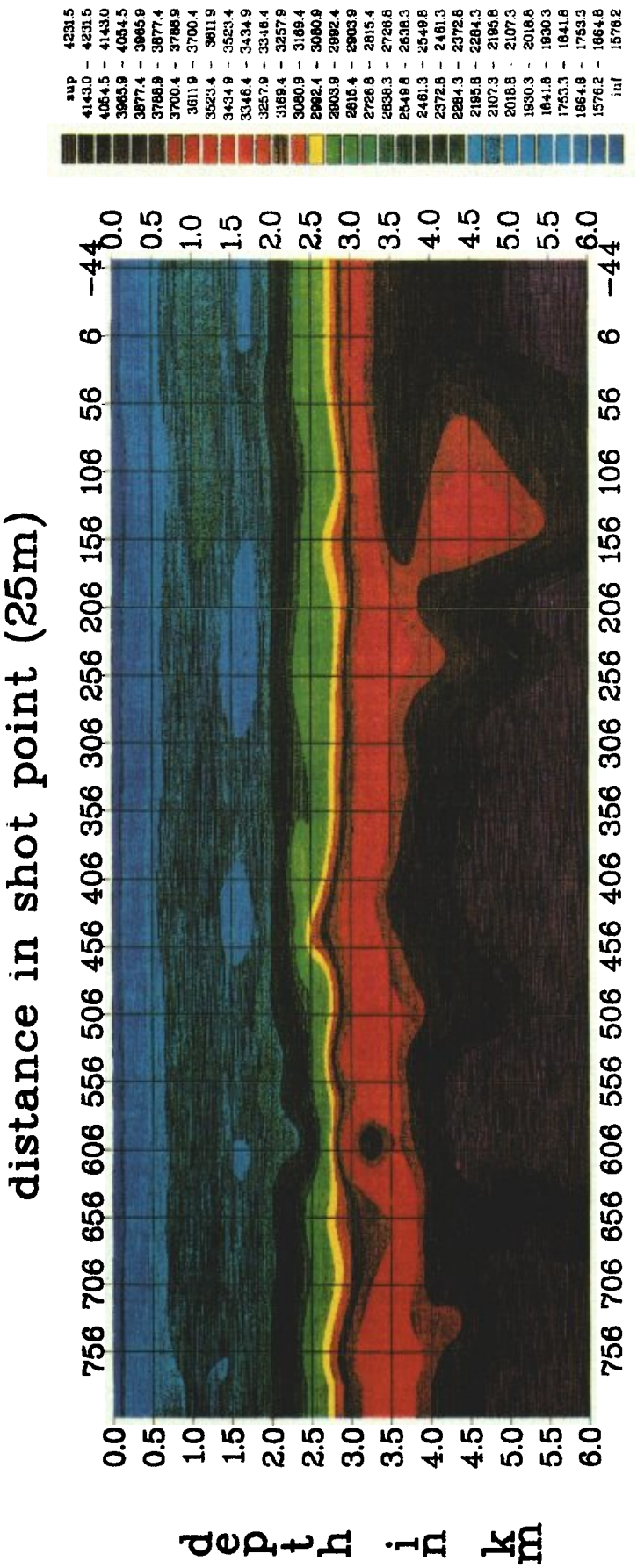

FIG. 8. Background velocity model for the Oseberg Field profile selected for asymptotic inversion. Velocities were obtained by standard velocity analysis provided to us together with the data set.

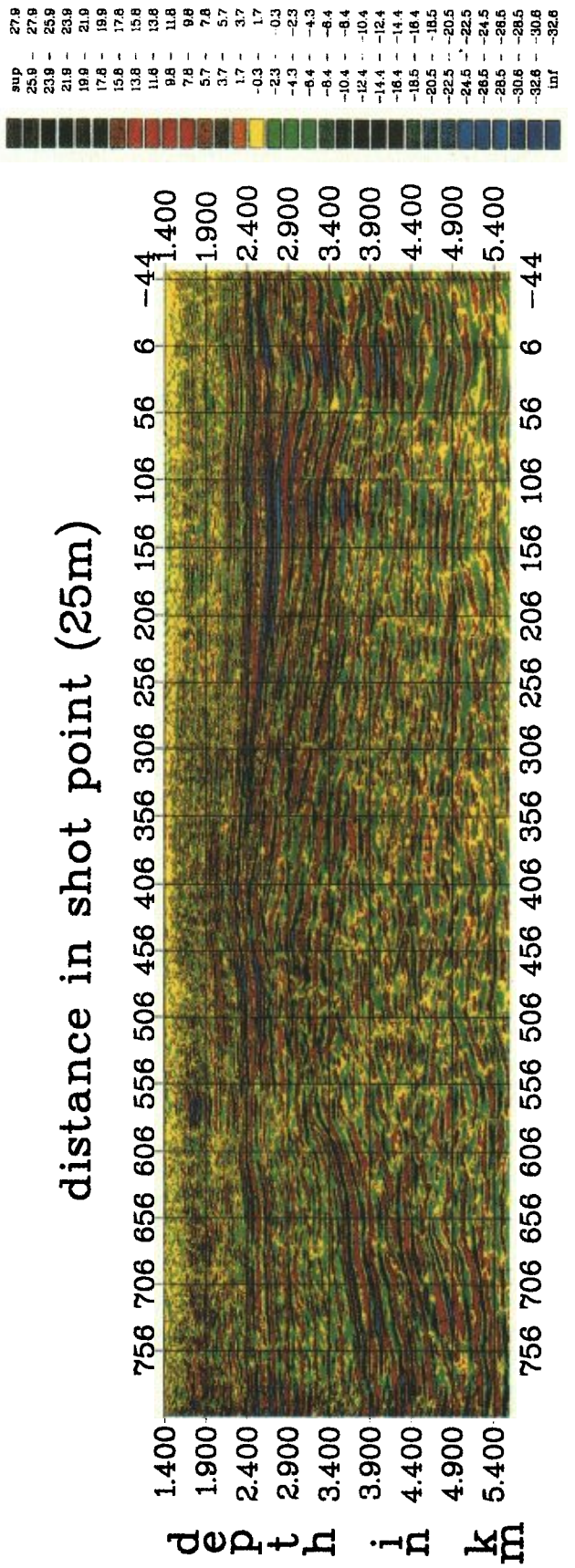

FIG. 9. Velocity perturbation for the complete Oseberg profile obtained after a single iteration of the asymptotic inversion in the "2.5-D" approximation. Seismograms from every eighth source were used in the inversion.

asymptotic inversion. We traced rays for all the selected sources and the 96 associated receivers, and we kept the results for the inversion procedure. Figure 9 gives us the migrated image in terms of velocity perturbation with respect to the depth. This image is similar to the one obtained by 3-D finite-difference migration and shows us the tilted block toward the Viking graben, as well as bright interfaces. Water multiples are still present and, somehow, complicate the interpretation of the migrated section. Obvious destructive interference between the source 240 and the source 360 would require another background velocity. We did not try to modify the reference medium, and we stopped at this first iteration for the whole profile. Other iterations would have introduced a higher frequency content in the image as we obtained for the well-defined target we will analyze now.

For stratigraphic interpretation—especially on how the Brent Group ends below the Cretaceous layer—an area drew our attention. We decided to test the performance of the iterative method for this subset of the data where 250 shots were involved. The first iteration, which is a small section of the complete profile of Figure 9, is presented on the top panel of Figure 10, while the second and third iterations are on the two other panels. The high-frequency content of the migrated image increases with the order of iteration, while the residues for the first two iterations decrease significantly. The second and the third sections are quite similar, leading us to assume that convergence was reached.

Stratigraphic interpretation is still difficult, especially for the top of the Brent Group between sources 330 and 380, but we find that the prolongation of the reflector related to the top of the Brent Group is unambiguously defined below the Cretaceous interface (Figure 10).

To estimate the quality of the inverted images, we calculated the variance (or energy) of the data ($E_{data} = \|data\|^2$) and of the residues. We then calculated the residual energy reduction (RER) by the following expression $RER = 100(1 - E_{residue}/E_{data})$. The value of RER decreased from 80 percent at the outcome of the first iteration down to about 70 percent at the end of the third iteration. From residues for a given shot as shown in Figure 11, it is easy to see that the RER does not steadily decrease with iterations because of unexplained local energy. The iterative asymptotic inversion has successfully explained most of the reflections by velocity perturbations in spite of the restrictions associated with the Born approximation. Let us recall, however, that we assumed acoustic propagation; therefore any converted phases between compressional and shear waves will be interpreted as $P - P$ reflections. One has to be aware of this limitation when looking at the subsurface image.

A better test of the inversion results is provided by well number 36/10 drilled down to 2500 m near shot 350, right in our target area. As shown in Figure 12, we convolved the profiles of velocity and impedance along the borehole with a wavelet to bring these profiles to the same spatial resolution of the seismic source. We compared the filtered profiles with those obtained from our inversion method at the shot points 350 to 356 located very close to the borehole. As shown in Figure 12, the agreement between the inverted and filtered profiles is excellent, both for velocity and impedance. Two main reflectors are clearly identified in the inverted image. This final test makes us confident that our algorithm produced valid images of the earth subsurface.

Another test of the quality of the inversion and the suitability of the background velocity model are the Iso-X profiles defined previously. The Iso-X profile in Figure 13 was calculated under the shot point number 401. Lateral continuation of the inverted impedance profiles is an excellent indication of the quality of the background velocity and also of the stability and quality of the wave propagation method.

Concerning computational efficiency, we found that tracing a single ray takes between 15 and 30 s of CPU time of a CRAY-XMP, depending on the number of horizons used in the ray-field continuation method. Constructing the image of a single point takes less than 1 s per iteration, so that the most expensive part of our program is ray tracing. Any further efforts to reduce the CPU time required for ray tracing is therefore most welcome.

CONCLUSIONS AND DISCUSSION

We demonstrated that a linearized inversion procedure based on the classical theory of optimization as proposed in Tarantola (1987) and coworkers, and using several important results from the asymptotic inversion theory proposed in Beylkin (1985) leads to a fast and efficient algorithm for linearized inversion. Our method—entirely based on the consistent use of ray theory for the calculation of seismograms, gradients, and Hessians—is an efficient alternative to inversion based on finite-difference modeling of the wave equation.

For a long, complex seismic profile from the Oseberg field in the North Sea, we showed that we could handle realistically sized seismic profiles with *presently available computers*. We also showed with several tests that we could correctly explain most of the signal in a profile using ray theory. The main difficulty with the application of ray theory is the sheer number of rays that would be required if we tried to trace rays from every point in the medium to each source and receiver. To accelerate seismic field computations we developed an original method for the depth continuation of a wavefield by rays.

The results of linearized inversion were successfully compared with well logs available from the area of the seismic profile. The coherency of the image and the validity of the reference model that we determined by classical velocity analysis were verified by a set of Iso-X sections. A total reduction of about 30 percent of the variance of the data was obtained at the end of three iterations in the inversion of a subset of the Oseberg data. This reduction in variance may not be very significant, though, because most of the energy of the residuals is concentrated near the borders of the profile and near the muted arrivals.

Our experience shows, that as long as the background model does not differ much in its spatial low-frequency components from the expected final model, the accuracy of the recovered image improves significantly when iterations are performed. Of course, when one has a final image, it is always possible to smooth it and start the whole procedure again with a new background. We have not performed this

(text continued on p. 1153)

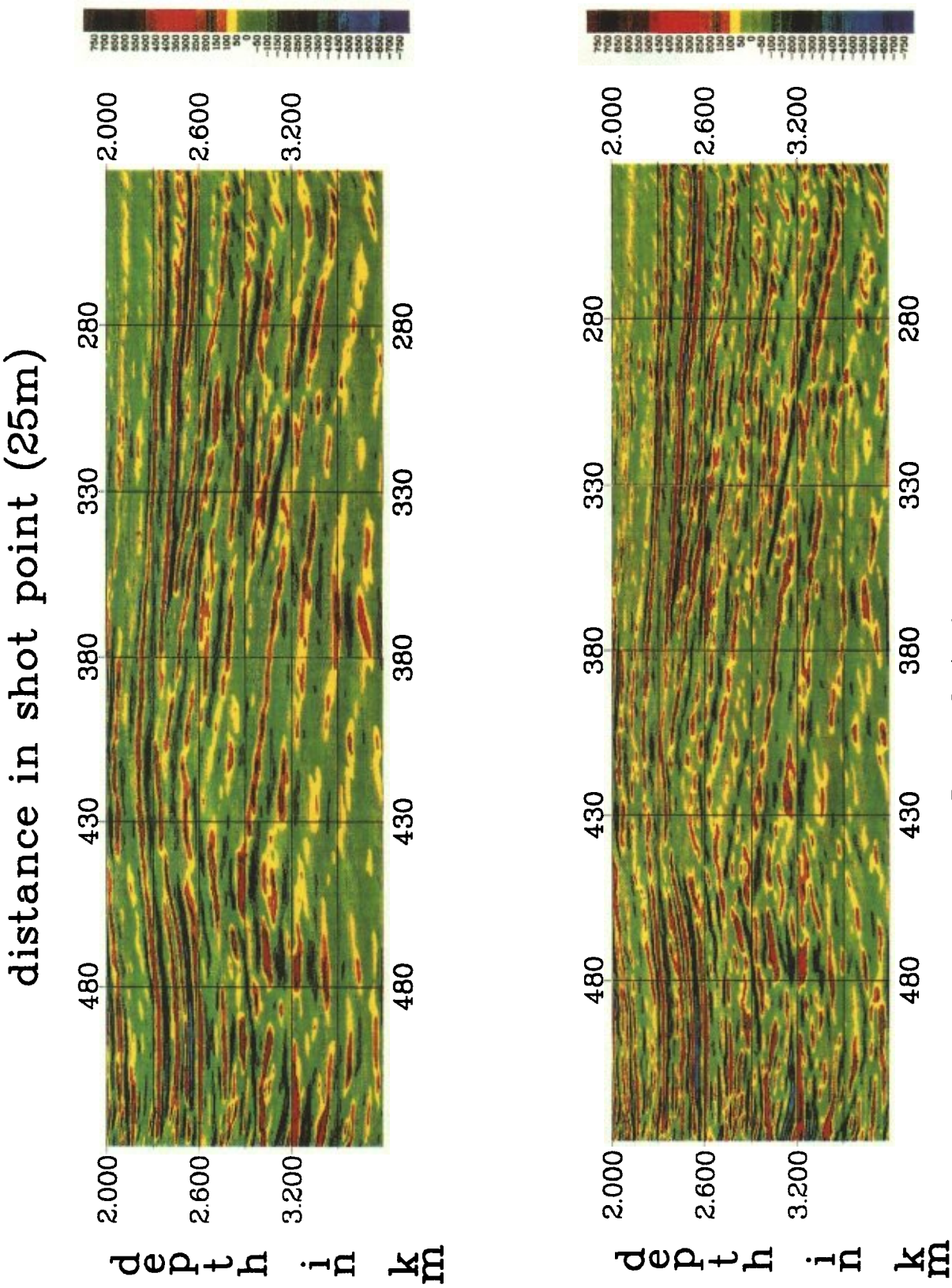

FIGURE 10. Continued on next page.

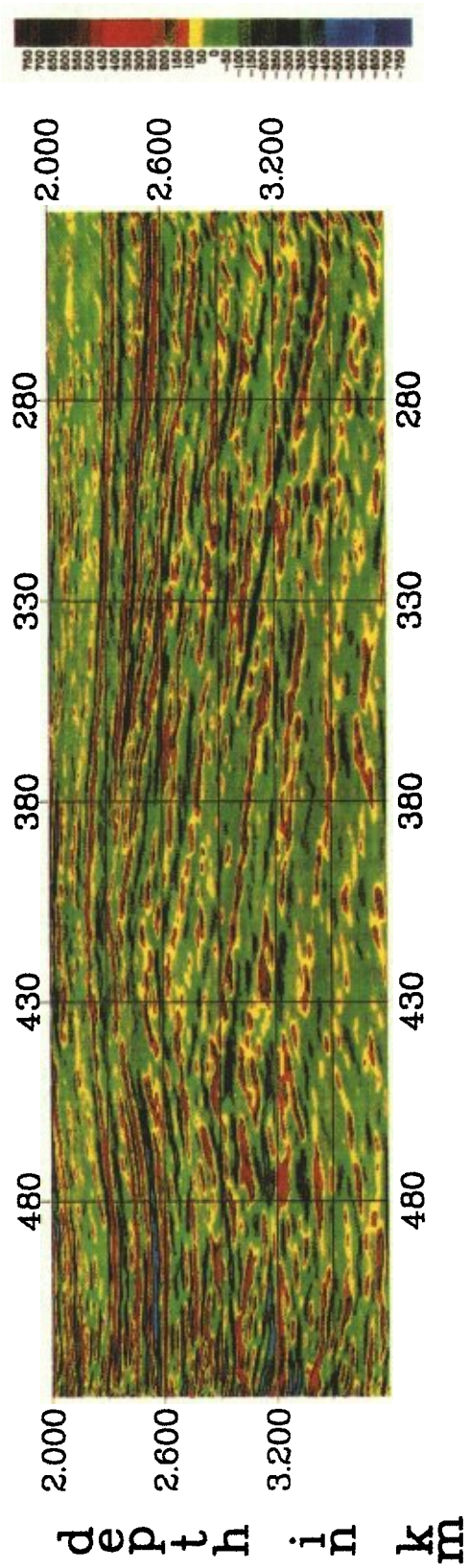

FIG. 10. Velocity perturbations inverted in the smaller target zone of the Oseberg profile; the succesive iterations are shown in the different panels.

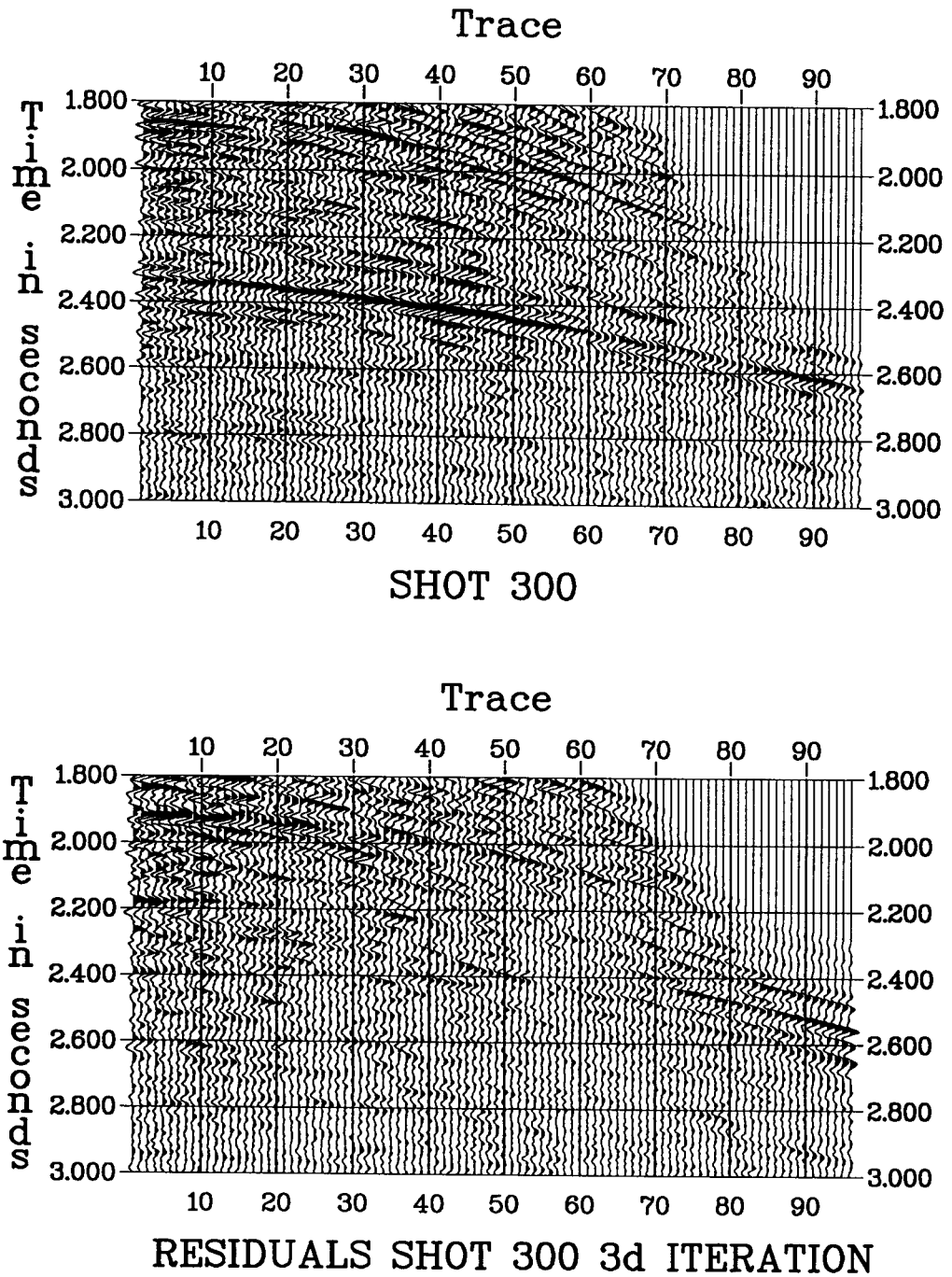

FIG. 11. Seismograms and residuals for one of the shot points used to invert the velocity under the target zone. Note the successful removal of reflections as shown by the residuals, although the procedure fails in some local areas.

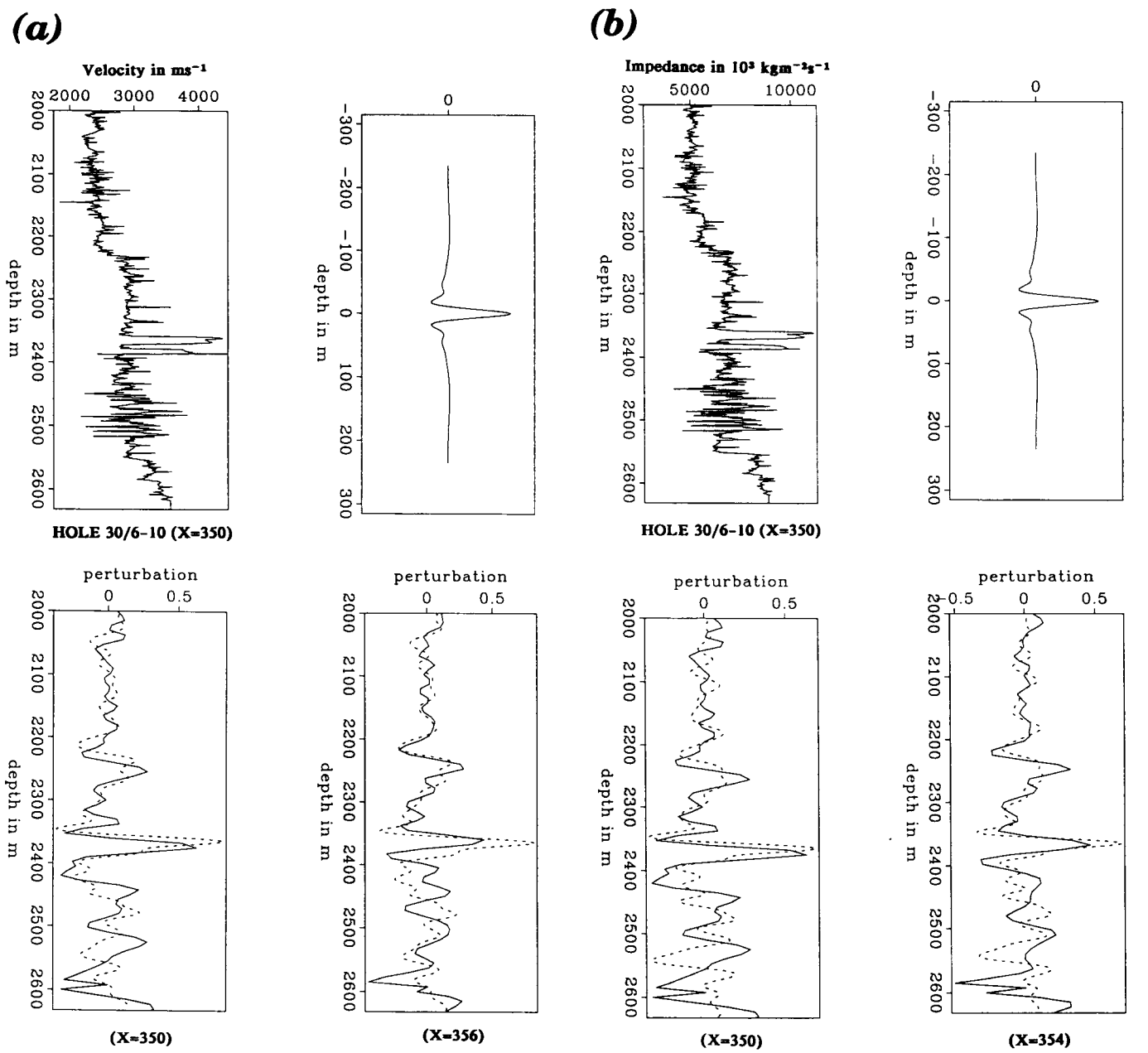

FIG. 12. (a) Comparison between the seismic velocity log at well 36/10, which is located near $x = 350$ and the results of asymptotic inversion. The original log, shown in the top left panel, was convolved with the Ricker wavelet shown at the top-right panel. In the two panels at the bottom, we compare the results of the inversion (full lines) with the filtered logs (dotted lines) at two neighboring horizontal positions. (b) Comparison between the seismic impedance log at well 36/10 convolved with a Ricker wavelet and the impedance perturbation inverted for the same horizontal position. See comments for (a) for a description of the panels.

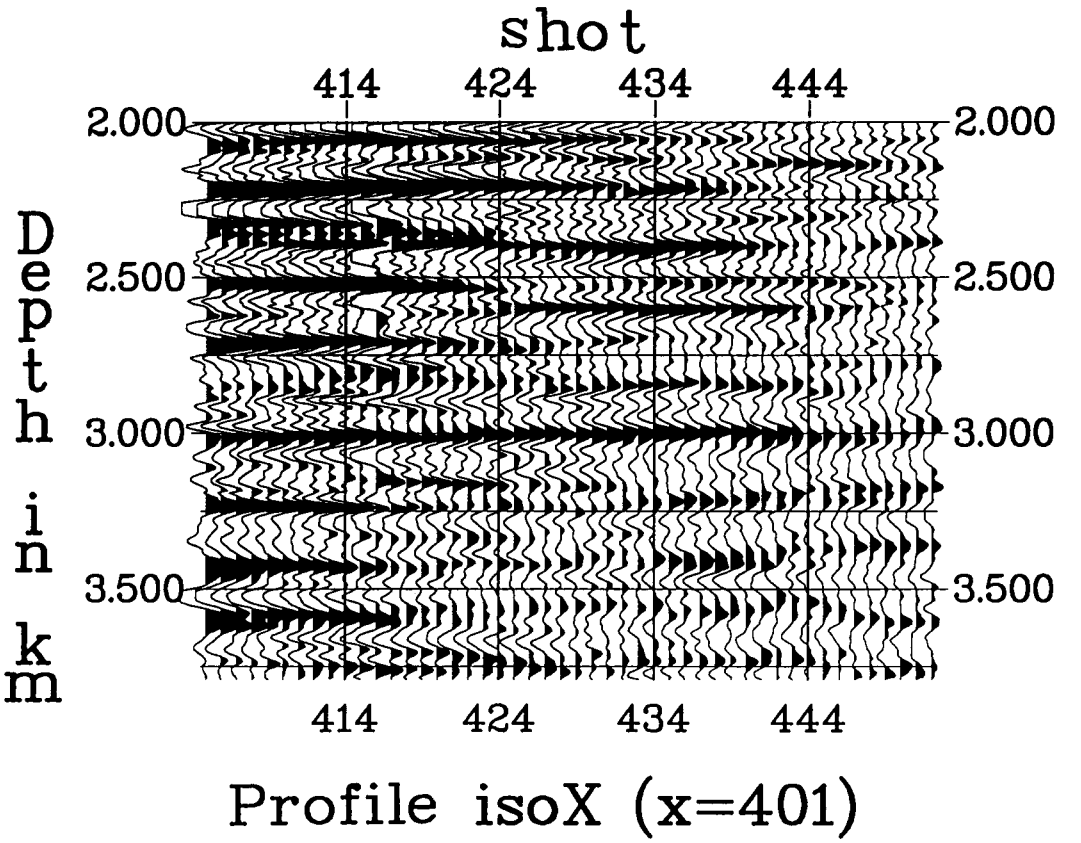

FIG. 13. Iso-X section computed at horizontal position x = 401. For the correct background velocity, reflectors must appear as horizontal arrivals in an Iso-X section. This is clearly the case in this Figure; this is an important argument in favor of the quality of the background model and linearized inversion.

nonlinear iteration because the retrieval of low spatial frequencies from linearized inversion is not particularly good. As is well known, reflectivity is controlled by the frequency contents of the source signal, while the traveltimes are controlled by the long wavelength part of the background velocity. It is therefore difficult to estimate a velocity model in the intermediate spatial frequency band between these two extremes.

From a practical point of view, the iterative asymptotic inversion could be focused on a particular area of the seismic profile where a very accurate image may be required for seismic interpretation. We hope that this technique will enable the construction of correct images beneath well-deformed 2-D structures.

In conclusion, we demonstrated that our algorithm could handle large amounts of field data. We also showed from the Oseberg data that the iterative asymptotic inversion can help in the detailed analysis of seismic sections.

ACKNOWLEDGMENTS

This work was supported by the Groupement de Recherche "Sismique" established by CNRS, IFP, and Elf Aquitaine (SNEAP). The Oseberg data was provided to us by SNEAP, and computer time was partially provided by IFP. We thank F. Chapel, P. Esquier, and P. Thore for interesting and constructive discussions on the Oseberg data. We are particularly indebted to V. Richards of IFP for his continuous support and his help in interpreting the well-log using the IFP's Interwell software. Contribution IPG No. 1199.

REFERENCES

Badley, M. E., Egeberg, T., and Nipen, O., 1984, Development of rift basins illustrated by the structural evolution of the Oseberg feature, Block 30/6, offshore Norway: J. Geol. Soc., **141**, 639–649.

Beylkin, G., 1985, Imaging of discontinuities in the inverse scattering problem by inversion of a causal generalized Radon transform: J. Math. Phys., **26**, 99–108.

Beylkin, G., and Burridge, R., 1990, Linearized inverse scattering problems in acoustics and elasticity, Wave Motion, **12**, 15–52.

Bleistein, N., 1987a, Two- and one-half dimensional Born inversion with an arbitrary reference: Geophysics, **52**, 26–36.

——— 1987b, On the imaging of reflectors in the earth, Geophysics, **52**, 931–942.

Červený, V., 1987, Ray-tracing algorithms in three-dimensional laterally varying layered structures, *in* Nolet, Ed., Tomography in seismology and exploration seismics: D. Reidel Publ. Co.

Červený, V., Molotkov, I. A., and Pšenčík, I., 1977, Ray method in seismology: Charles Univ. Press.

Cohen, J. K., and Bleistein, N., 1977, An inverse method for determining small variations in propagation speed: SIAM J. Appl. Math., **32**, 784–799.

Crase, E., Pica, A., Noble, M., McDonald, J., and Tarantola, A., 1990, Robust elastic nonlinear waveform inversion: Application to real data: Geophysics, **55**, 527–538.

Farra, V., Virieux, J., and Madariaga, R., 1989, Ray perturbation theory for interfaces, Geophys. J. Int., **99**, 377–390.

Gauthier, O., Virieux, J., and Tarantola, A., 1986, Two-dimensional nonlinear inversion of seismic waveforms, numerical results: Geophysics, **51**, 1387–1403.
Hanyga, A., 1988, Numerical tracing of rays and wavefronts, *in* Doornbos, D. J., Ed., Seismological algorithms: Academic Press Inc.
Jin, S., Madariaga, R., Virieux, J., and Lambaré, G., 1992, Two-dimensional asymptotic iterative elastic inversion: Geophys. J. Int., **108**, 575–588.
Kolb, P., Collino, F., and Lailly, P., 1986, Prestack inversion of 1-D medium: Proc. IEEE, **74**, 498–508.
Lambaré, G., 1991, Inversion linéarisée de données de sismique réflexion par une méthode quasi-newtonienne: Thèse, Université Paris 7, Paris.
Miller, D., Oristaglio, M., and Beylkin, G., 1987, A new slant on seismic imaging: Migration and integral geometry: Geophysics, **52**, 943–964.
Mora, P., 1987, Nonlinear two-dimensional elastic inversion of multioffset seismic data: Geophysics, **52**, 1211–1228.
Nipen, O., 1987, Oseberg *in* Spencer, A. M., Ed., Geology of the Norwegian oil and gas fields: Graham & Trotman, Ltd.
Pica, A., 1988, Inversion nonlinéaire de formes d'ondes en sismique réflexion, Application sur des données réelles à offset: Thèse, Université Paris 7, Paris.
Pica, A., Diet, J. P., and Tarantola, A., 1990, Nonlinear inversion of seismic reflection data in a laterally invariant medium: Geophysics, **55**, 284–292.
Snieder, R., Xie, M., Tarantola, A., and Pica, A., 1989, Retrieving both the impedance contrast and the background velocity: A global strategy for the seismic reflection problem: Geophysics, **54**, 991–1000.
Tarantola, A., 1984, Inversion of seismic reflection data in the acoustic approximation: Geophysics, **49**, 1259–1266.
——— 1987, Inverse problem theory: Methods for data fitting and model parameter estimation: Elsevier Science Publ. Co., Inc.
Virieux, J., 1984, *SH*-wave propagation in heterogeneous media: Velocity-stress finite-difference method: Geophysics, **49**, 1933–1957.
Virieux, J., Farra, V., and Madariaga, R., 1988, Ray tracing in laterally heterogeneous media for earthquake location: J. Geophys. Res., **93**, 6585–6599.